Modeling and Realization of Photovoltaic Simulator Based on a Buck DC-DC Converter

Navid Reza Abjadi[1]

Abstract: This paper presents a simple accurate model for photovoltaic (PV) modules suitable for implementation by digital signal processors (DSPs). A buck DC-DC converter is employed to realize the PV characteristic appropriately. Three controllers set forth for current control according to PV voltage to achieve fast and accurate convergence. Computer simulation results are presented to investigate the effectiveness of the proposed PV system. Moreover, a practical setup is made and the proposed method using the obtained model for different temperatures and solar irradiations is tested in MATLAB/Simulink environment.

Keywords: PV module, PV modeling, PV simulator, Solar panel, Buck DC-DC converter.

1 Introduction

Solar energy plays an important role to generate electricity in the recent years because it is infinite, clean and friendly in environment. PV modules or solar panels are used more and more recently because of increasing electricity demand and environment concerns. There are many interests in PV modules in different research fields: modeling, control, connecting to battery or grid [1], maximum power point tracking (MPPT), PV shading [2] and etc. PV modules consist of many solar cells which are solid state devices. Nonlinear i-v characteristic of PV modules is considered in many research papers to obtain accurate models for various simulation software packages [3]; however, these models are not suitable for digital PV simulator or their implementation is difficult in real time systems; since, there are many constants and variables in these models. In [4], one of these models is introduced and a PV module is implemented using voltage buffering technique. This technique is not suitable for PV module with high powers because of huge power loss in the simulator. Switching DC-DC converters are usually used for diverse power conversion systems. They can be used for implementation of PV module simulator with high efficiency especially in high power. The buck or buck-boost converters can be used for such purpose; however, the boost converter is not suitable for PV simulator implementation, because it is a voltage

---

[1]Faculty of Engineering, Shahrekord University, Shahrekord, Iran; E-mail: navidabjadi@yahoo.com

step up converter; but, in a PV simulator the voltage needs to be reduced to zero for a short circuit. In [5 − 9] based on electrical models of solar cells namely ideal model, single diode model and double diode model, the PV module behavior is investigated and simulated in MATLAB/Simulink environment. The equations and their parameters are quit complex. In [10] artificial neural network (ANN) based simulation and experimental verification of analytical four and five parameters models of PV modules are presented.

PV module simulator can simplify researches in many solar panel researches and designs. Doing theses researches and designs in real world with real solar panel causes many difficulties; for example, the temperature and irradiation are not expectable and cannot be changed arbitrarily. [11] proposes a PV simulator based on a buck DC-DC converter in the PSIM software using the single-diode model. In [12] the PV simulator is realized using a push-pull DC-DC converter which has a more complicated dynamics compared with the buck converter but it can be used for more power generation. The PV simulator of [12] is implemented on a personal computer (PC). In [13] a real time photovoltaic simulator is designed, developed and implemented based on the single diode model of solar cells. A PV simulator is proposed in [14] using a constant current source and array of diodes. In [15], a double loop PI controlled buck converter is used as a PV simulator and the effect of wind speed is also considered in PV reference model which is not very essential in most of the PV system tests. In [16] a PV emulator is realized using a buck converter with a dSPACE controller which is rather expensive. This paper does not design any controller and the command pulses are generated by comparison of voltage error and a triangle signal. The obtained results represent oscillatory response near the open circuit and short circuit points. In [17], a synchronous buck converter is used as a PV simulator which fed by a boost converter. A double current mode control is used which needs both the inductor current and the load current. The proposed control method used in this paper also needs the input voltage and the controller is rather complicated. In addition, the i-v characteristics of the PV module is implemented by a large lookup table which occupy the memory of the DSP.

The purpose of the modeling in this paper is to obtain a simple i-v relation for each temperature and irradiation which is suitable in implementation with DSPs without any difficulty. Using switching strategy for implementation, high power PV modules can be simulated and large amount of power can be extracted to charge a battery or current injection to power grid with inverter.

The contributions of this paper are: presenting a simple model for PV module suitable for implementation in a DSP, presenting a simple low cost switching hardware with appropriate controls using the proposed model and designing and investigating three current controllers to realize the PV simulator. The stability issues of the system are checked and proved.

2 PV Module Model

The i-v characteristic of a PV module can be considered as two segments. The first segment is like a current source and the second segment which is the remain segment of the i-v curve can be approximated by a polynomial. To obtain this polynomial, data of current and voltage of the PV module is needed. The Data collection is done by a practical PV module or an available PV module in a simulation software such as PSIM or MATLAB. In this paper the data is obtained from PSIM as shown in diagram of Fig. 1. The i-v data can be obtained for different temperatures and solar irradiations. For each temperature and solar irradiation a polynomial is obtained. Using curve fitting technique for example in MATLAB software, the coefficients of the polynomial are obtained. After testing various polynomial degrees, a polynomial with 4th order degree is resembled the characteristic of the actual PV panel with a very good accuracy.
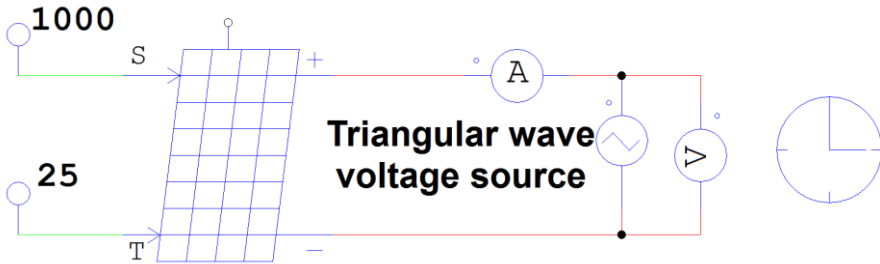

Fig. 1 – *PV module in PSIM software for obtaining i-v data.*

To show this claim, the i-v characteristic of three conditions namely 25°C-1000W/m^2, 50°C-1000W/m^2 and 25°C-500W/m^2 are plotted in Fig. 2. The obtained data from fitted 4th order polynomials is also plotted in Fig. 2 with ×, ○ and ∗ notations, respectively. From Fig. 2 it is seen that there is a very good accuracy in approximating i-v curve by a 4th order polynomial. Therefore, the model proposed for a PV module with a certain temperature and solar irradiation is as follow:

$$i = \begin{cases} I, & \text{for } v < V, \\ a_4 v^4 + a_3 v^3 + a_2 v^2 + a_1 v + a_0, \end{cases} \tag{1}$$

where I and V are positive constants obtained from the i-v curve and a_0 to a_4 are obtained coefficients from curve fitting.

It is worthwhile to note that the constant segment of the i-v curve should be considered separately to achieve a better accuracy and the polynomial coefficients should be obtained with adequate digits since the fitted 4th order polynomial is very sensitive with respect to coefficients.
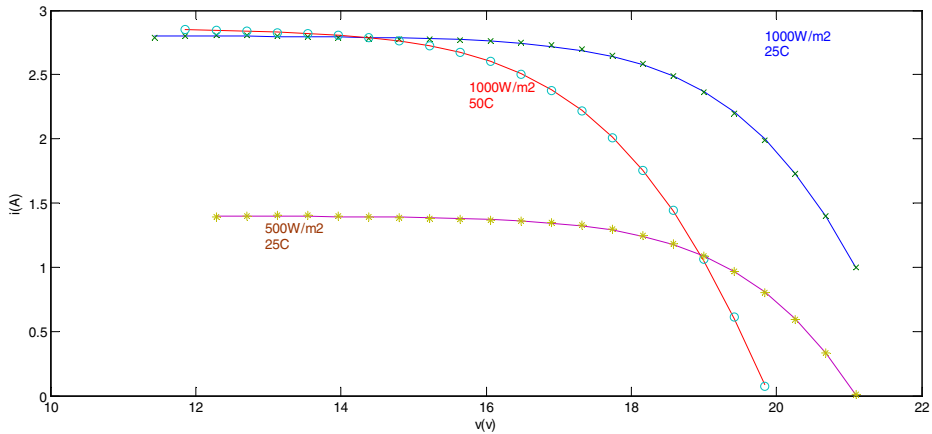
Fig. 2 – *The i-v characteristic of three conditions.*

3 PV Simulator Based on the Buck Converter

The schematic diagram of the proposed PV module simulator based on DC-DC buck converter is shown in Fig. 3. The data or the model equations of PV module characteristic are saved in the memory of a microcontroller or DSP. The output voltage is measured and based on the characteristic of the PV module, the reference output current is obtained. The actual output current is also measured by a current sensor such as a Hall effect sensor; then compared with its reference. In Fig. 3 two controls are proposed for current control. The first one is a simple comparator or relay which generates switch S pulses with variable frequency. The second one is a PI control plus PWM unit which generates switch S pulses with fixed frequency. The second control is more suitable for digital implementation because most of the DSPs have separate PWM unites. Using each of these controls, the error between output current and its reference converges to almost zero and the characteristic of the PV module is realized. Instead of the load R of Fig. 3, any other load or power converter can be used. The digital realization increases the versatility and programmability of the converter and the resulted PV module simulator.

It is assumed that the value of the inductor is large enough for the converter to operate in continuous conduction mode (CCM). This assumption causes that in addition to achieving a CCM, the inductor current ripple will also decrease and the inductor current will be approximately equal to the output current.
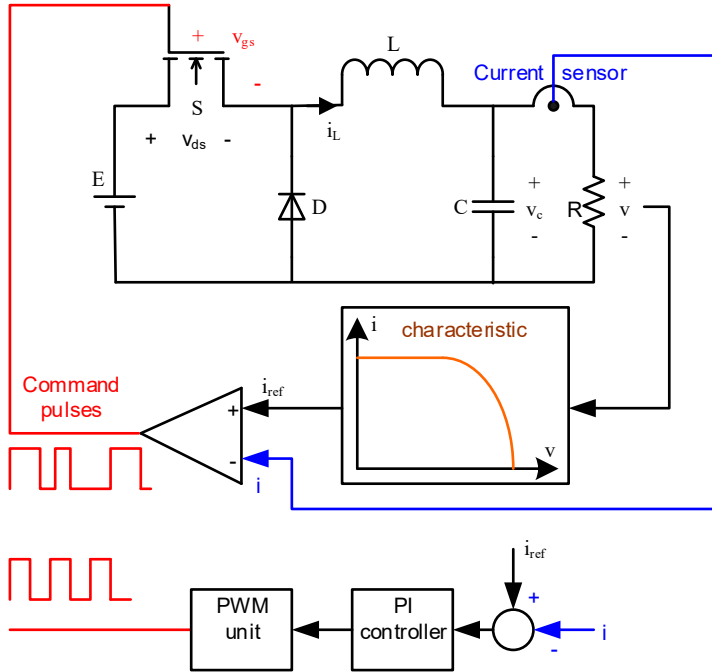
Fig. 3 – *Schematic diagram of the proposed PV module simulator.*

The differential equations of the buck converter in CCM are given by

$$L\frac{\mathrm{d}i_l}{\mathrm{d}t} = -v_C + Eu$$

$$C\frac{\mathrm{d}v_C}{\mathrm{d}t} = i_L - Gv_C, \tag{2}$$

where G is the electrical conductance of the load and u is the switch S command or control input ($u \in \{0,1\}$). When the switch S is off, $u = 0$ and when the switch S is on, $u = 1$.

The average model is obtained by substituting the discontinuous control input in (2) by a continuous control signal which is the average of the switch command. For notation simplicity, same notations are used for both instantaneous variables and average variables. If u considered as a continuous control signal ($0 < u < 1$), (2) can be considered as the average model.

Equation (2) can be rewritten as the following affine form:

$$\dot{x} = f(x) + g(x)u, \tag{3}$$

where $x^{\mathrm{T}} = [i_L \quad v_C]$,

$$\boldsymbol{f}(x) = \begin{bmatrix} -\dfrac{x_2}{L} \\ \dfrac{x_1}{C} - \dfrac{x_2}{RC} \end{bmatrix} \quad \text{and} \quad \boldsymbol{g}(x) = \begin{bmatrix} \dfrac{E}{L} \\ 0 \end{bmatrix}. \tag{4}$$

3.1 The first control: sign function

It is worthwhile to note assuming capacitance C is large enough, the inductor current i_L is almost equal to the output current i. The first control proposed in Fig. 3 is in fact a sliding mode (SM) control which is investigated more thoroughly.

Setting the time derivatives to zero, the equilibrium point of (3) is given by

$$\bar{\boldsymbol{x}} = (\bar{x}_1, \bar{x}_2) = (G\bar{x}_2, \bar{x}_2) = (\bar{x}_1, R\bar{x}_1), \tag{5}$$

where $\bar{x}_1 = i_{ref}$, and $\bar{x}_2 = Ri_{ref} = E\bar{u}$; $\bar{u}$ is the steady-state value of u at the equilibrium point.

Define the following output or sliding variable

$$h(x) = x_1 - \bar{x}_1. \tag{6}$$

The sliding surface is defined as

$$S = \{\boldsymbol{x} \in \Re^2 \,|\, h(x) = 0\}. \tag{7}$$

The direction derivatives or Lie derivatives of $h(\boldsymbol{x})$ with respect to $\boldsymbol{f}(x)$ and $\boldsymbol{g}(x)$ are [18, 19]

$$L_f h(x) = -\dfrac{x_2}{L}, \quad L_g h(x) = \dfrac{E}{L} > 0, \tag{8}$$

where

$$L_f h(x) \square \dfrac{\partial h}{\partial x} \boldsymbol{f} \quad \text{and} \quad L_g h(x) \square \dfrac{\partial h}{\partial x} \boldsymbol{g}.$$

In sliding mode control, the equivalent control u_{eq}, which restricts the state trajectory to S surface, is obtained by equating the time derivative of sliding variable $h(x)$ to zero considering nominal parameters. The equivalent control for the system (3) and the sliding variable (6) is obtained as follow [19]:

$$\dot{h}(x) = 0 \quad \Rightarrow \quad \dfrac{\partial h}{\partial t} = \dfrac{\partial h}{\partial x}\dot{\boldsymbol{x}} = 0, \quad \text{or}$$

$$\dfrac{\partial h}{\partial t}\big(\boldsymbol{f}(x) + \boldsymbol{g}(x)u_{eq}\big) = L_f h(x) + L_g h(x)u_{eq} = 0,$$

which yields

$$u_{eq} = -\frac{L_f h(x)}{L_g h(x)} = \frac{x_2}{E} . \tag{9}$$

Since $0 < x_2 < E$, one concludes $0 < u_{eq} < 1$ which is the necessary and sufficient condition for existence of a sliding regime [19].

Considering the fact that $L_g h(x) > 0$, using the following control law, the state trajectories hit the sliding surface S which yields the desired regulation [19].

$$u = \begin{cases} 1 & if \quad h(x) < 0 \\ 0 & if \quad h(x) > 0 \end{cases} = \frac{1}{2}\left[1 - \text{sign } h(x)\right]. \tag{10}$$

The ideal sliding dynamics is given by

$$\dot{x} = f(x) + g(x)u_{eq}, \tag{11}$$

which coincides the zero dynamics ($y = h = 0$).

Considering the system (3), the second equation of the system is not used, therefore, the internal dynamics is $\dot{x}_2 = \frac{x_1}{C} - \frac{x_2}{RC}$. The zero dynamics is obtained, considering $y = h = 0$ in internal dynamics

$$\dot{x}_2 = \frac{\bar{x}_1}{C} - \frac{x_2}{RC} = \frac{\bar{x}_2 - x_2}{RC} . \tag{12}$$

Consider the following Lyapunov function

$$V(x_2) = \frac{1}{2}(x_2 - \bar{x}_2)^2 . \tag{13}$$

Taking the derivative of (13) with respect to time and substituting from (12), one can obtain

$$\dot{V}(x_2) = -\frac{1}{RC}(x_2 - \bar{x}_2)^2 , \tag{14}$$

which is a negative definite function and yields the asymptotically stability of the equilibrium point.

3.2 The second control: PI control

Consider the second control proposed in Fig. 3. Assuming the switching frequency of the PWM unit is large enough that one can abandon the effect of the PWM unit. Consider (2) as converter average model, the following transfer function between control input u and output current i is obtained

$$\frac{I(s)}{U(s)} = \frac{GE}{LCs^2 + LGs + 1}, \tag{15}$$

where s is the Laplace transform variable; $I(s)$ and $U(s)$ denote Laplace transforms of the corresponding variables.

The transfer function of the PI controller is given by

$$\frac{U(s)}{E(s)} = K_p + \frac{K_i}{s},$$ (16)

where $E(s) = I_{ref}(s) - I(s)$ and $I_{ref}(s)$ is the Laplace transform of the reference current.

Combining (15) and (16), one can obtain the closed-loop transfer function as

$$\frac{I(s)}{I_{ref}(s)} = \frac{GE(K_p s + K_i)}{LCs^3 + LGs^2 + (1 + GEK_p)s + GEK_i}.$$ (17)

The coefficients of the denominator of (17) are positive and with proper choice of K_p and K_i a stable closed-loop system with satisfactory step response is achieved. The DC gain of (17) is equal to 1; in fact, the integral action eliminates the steady-state error for step reference input.

3.3 The third control: nonsingular terminal sliding mode control

Terminal sliding mode (TSM) control is an improved SM control in which the sliding variable contains fractional order. There are two phases in SM control: the reaching phase and the sliding phase. Using TSM control both of these phases can terminated in finite times. In [20], a nonsingular terminal sliding mode (NTSM) controller is introduced which is a fast and effective controller and does not have the singularity problem of conventional TSM controllers. The NTSMC of [20] is employed here to design a novel current control for PV simulator.

Consider the state space equations in (3) – (4) and the following new variables:

$$y_1 = \int \left(x_1 - \bar{x}_1 \right) dt,$$ (18)

$$y_2 = x_1 - \bar{x}_1.$$ (19)

Using the variables defined in (18)–(19), the state space equations can be rewritten as

$$\dot{y}_1 = y_2,$$
$$\dot{y}_2 = \dot{x}_1 - \dot{\bar{x}}_1 = f_1 + g_1 u + \Delta - \dot{\bar{x}}_1,$$ (20)

where Δ is the lumped uncertainties and disturbances.

The NTSM control sliding variable is chosen as [20]:

$$s = y_1 + \beta^{-1} y_2^{p/q},$$ (21)

where β is a positive constant and p and q are positive odd numbers satisfying $p > q$. In Appendix 2, it is shown that using the sliding variable (21), the sliding phase occurs in finite time.

Taking the time derivative of (21) and using (20), yields

$$\dot{s} = \dot{y}_1 + \beta^{-1}\frac{p}{q}y_2^{\frac{p}{q}-1}\dot{y}_2 = y_2 + \beta^{-1}\frac{p}{q}y_2^{\frac{p}{q}-1}\left[f_1 + g_1 u + \Delta - \dot{\bar{x}}_1\right]. \qquad (22)$$

Using nominal parameters (without considering the uncertainties and disturbance: $\Delta = 0$) and equating $\dot{s}$ from (22) to 0, gives

$$u_{eq} = \frac{-\beta\frac{q}{p}y_2^{2-\frac{p}{q}} - f_1 + \dot{\bar{x}}_1}{g_1}. \qquad (23)$$

The NTSM control law can be written as (see Appendix 1) [20]

$$u = u_{eq} + u_{reach}, \qquad (24)$$

where

$$u_{reach} = -\eta\,\text{sign}(s)/g_1.$$

Instead (24), one can use the following control law which is easier to implement [19].

$$u = \frac{1}{2}[1 - \text{sign}(s)]. \qquad (25)$$

4   Computer Simulation

Fig. 4. shows the simulation block diagram of the proposed PV module simulator with PSIM software. In this simulation, the PV module is in parallel with the buck converter and both of them are connected to a voltage source with a triangular waveform to sweep the voltage in a wide range of the system operation. The output voltage of the buck converter is equal to the voltage of the PV module; thus the current of the PV module is measured and used as reference current of the buck converter. Using this technique in simulation, the buck converter behaves similar to the PV module.

Table 1 shows the parameters of the buck converter. The PV module specifications are also given in **Table 2**.

The obtained simulation results are illustrated in Figs. 5 – 8. The solar irradiation is changed from 2000 W/m^2 to 1000 W/m^2 at $t = 0.02$ s. The results for triangular sweep voltage is represented in Fig. 5 and Figs. 6, 7 and 8 show the resulted currents for PI control, SM control and NTSM control respectively.
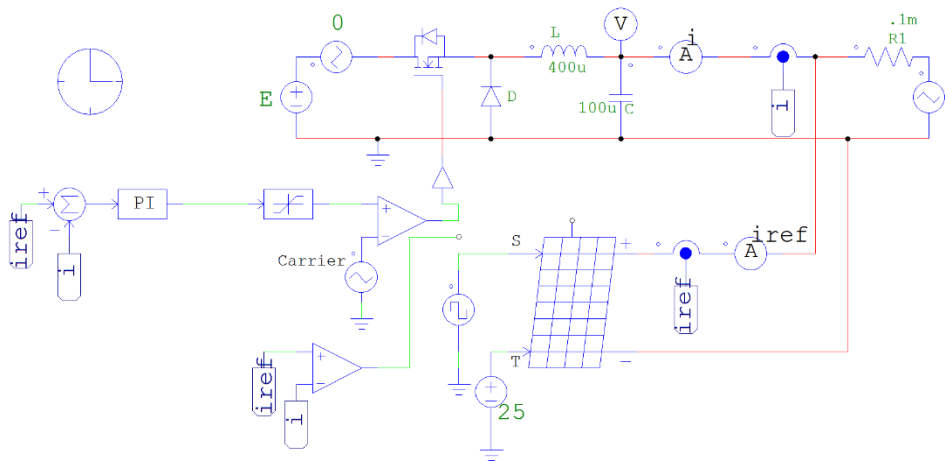
Fig. 4 – *The simulation block diagram with PSIM.*

Table 1
The parameters of the buck converter.

Inductance *L*	400 µH
Capacitance *C*	100 µF
Input voltage *E*	30 V
Switching frequency	20 kHz

Table 2
PV module specification.

Number of cells	38
Maximum power	47 W
Voltage at maximum power with reference cell temperature and standard light	18.2 V
Open circuit voltage	21.6 V
Reference cell temperature	25 °C
Standard light intensity at 25 °C	1000 W/m^2
Current at maximum power	2.6 A
Short circuit current	2.8 A
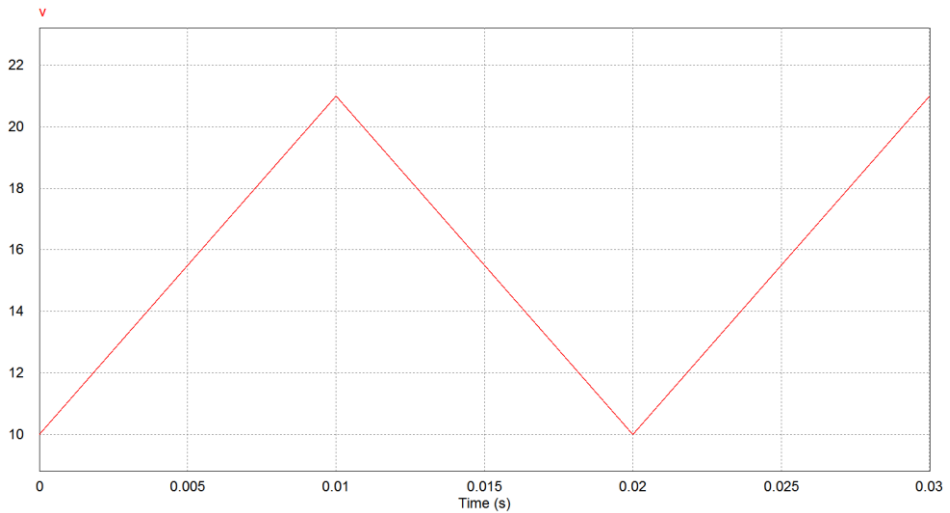
Fig. 5 – *The simulation results for triangular sweep voltage.*
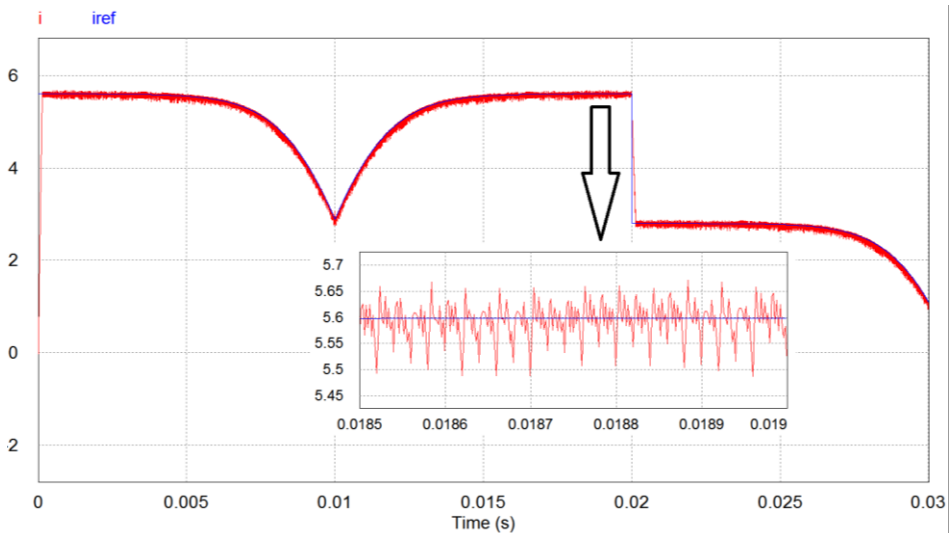
Fig. 6 – *The simulation results of output current and its reference for PI control.*

It is seen that compared to PI control the obtained result for SM control is more coincide the reference current and compared to SM control the obtained result for NTSM control is more coincide the reference current; however, the frequency of the sign functions in SM control and NTSM control are variable and these methods are more suitable for analog implementation with Op-Amps to achieve high switching frequencies. A fixed frequency version of SM control and NTSM is also achievable. To show the effectiveness of the proposed PV

157

simulator with the first control method, another simulation is performed where the PV simulator is connected to a boost converter. The simulation results are shown in Fig. 9. In this simulation the duty cycle of the boost converter is 0.5 and the parameters of the boost converter are chosen same as the buck converter used in PV simulator given in **Table 1**. The solar irradiation is changed from 1200 W/m^2 to 400 W/m^2 at $t = 0.02$ s . The simulation results illustrate that the stability is preserved and the output current of the PV simulator tracks its reference perfectly.
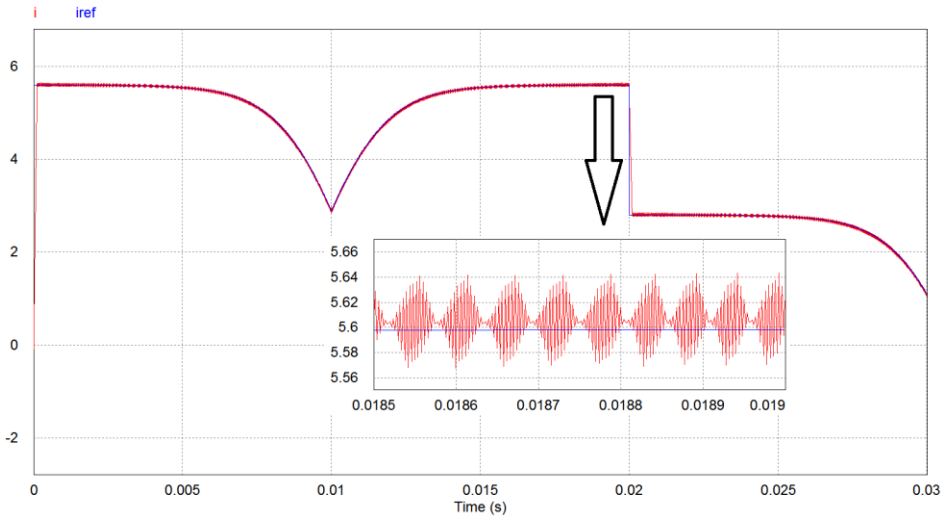
Fig. 7 – *The simulation results of output current and its reference for SM control.*
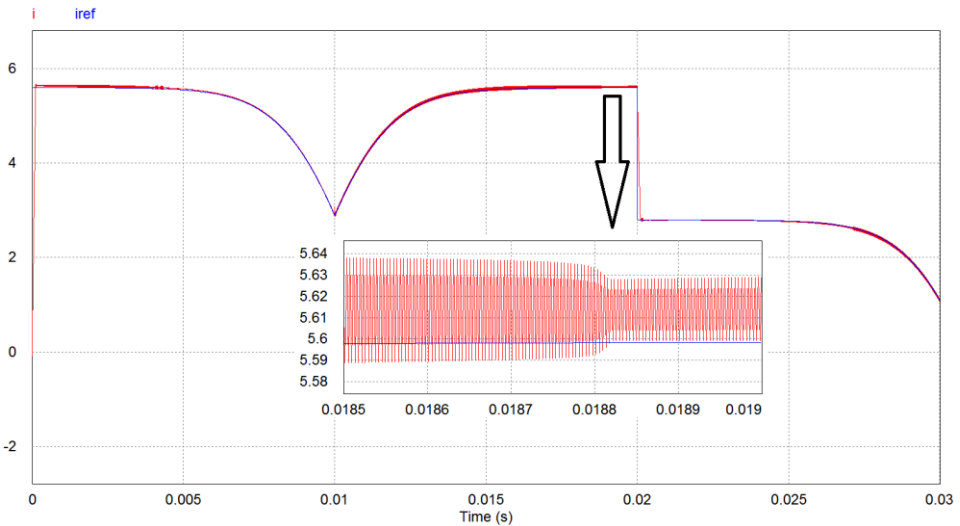
Fig. 8 – *The simulation results of output current and its reference for NTSM control.*
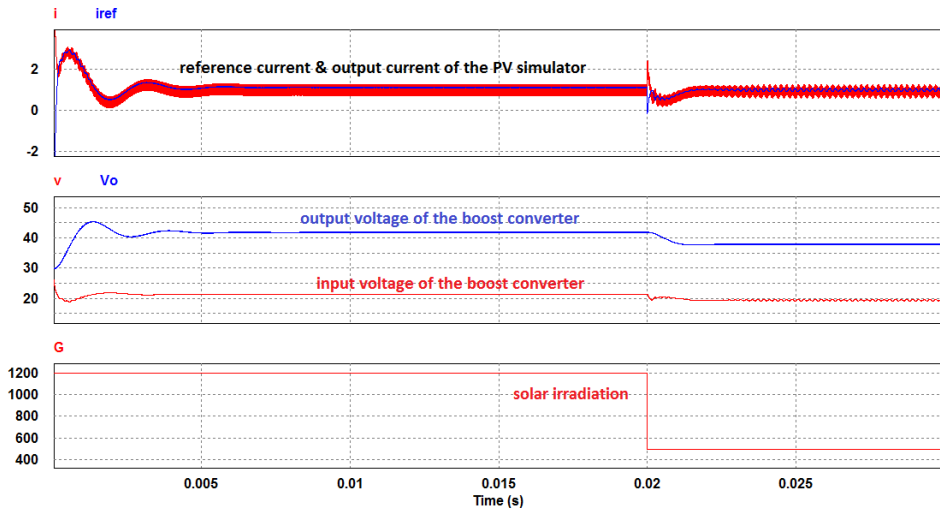
158

Fig. 9 – *The simulation results obtained with connection of a boost converter to the PV simulator.*

5 Experimental Results

Fig. 10 represents the experimental setup for realization of the proposed PV module simulator.

The buck converter parameters are the same as the ones given in the simulation section. The load connected to the simulator is changed between 25Ω and 12.5Ω with a power MOSFET on the load board. To measure the output current of the buck converter a Hall effect current sensor ACS712-5A is used. The PV module model obtained by curve fitting for several irradiation and temperature conditions is used in the SIMULINK software program and the generated codes are loaded to the DSP. The DSP is a low cost DISCOVERY STM32F407 microcontroller with 12-bits A/Ds and 168MHZ clock frequency. A sample of the gate-source and drain-source voltages of the buck converter MOSFET is given in Fig. 11 which show the perfect switching action of the buck MOSFET switch.

Three tests are considered in this section to show the validity and effectiveness of the proposed PV module simulator. The practical results presented are obtained by the first control method (sign function). The practical results presented are obtained by the first control method (sign function). This control has few calculations but is an effective method.

In the first test, the solar irradiation and temperature are kept on constant levels at 1000 W/m^2 and 25 $^\circ$C respectively and the load of the simulator is changed.

The obtained results are shown in Fig. 12. This figure shows the actual output current and its reference. The resistance of the load is changed between 25 Ω and 12.5 Ω periodically. It is seen the current tracks its reference perfectly with a good dynamic.
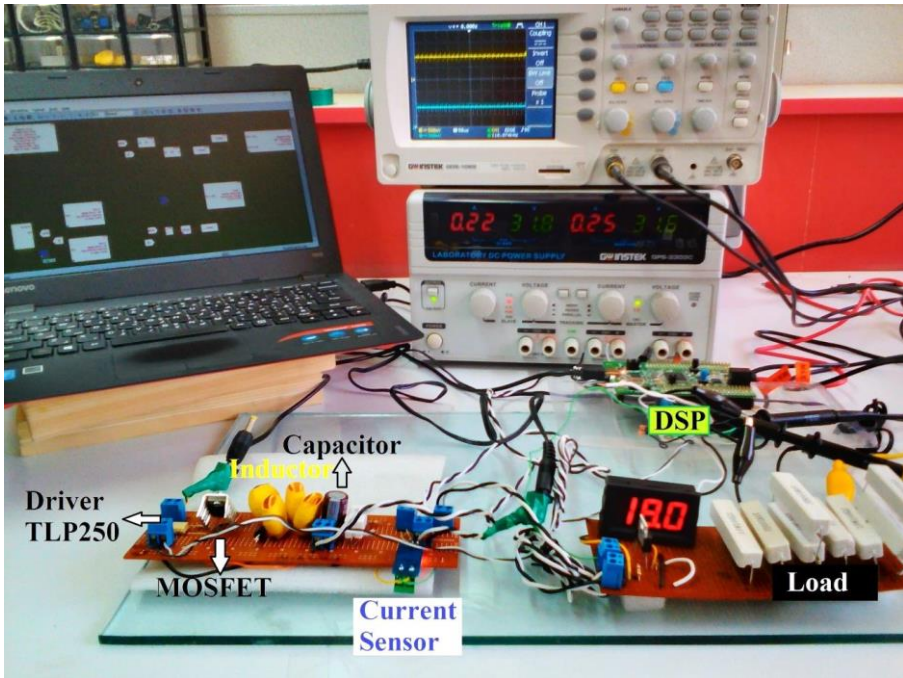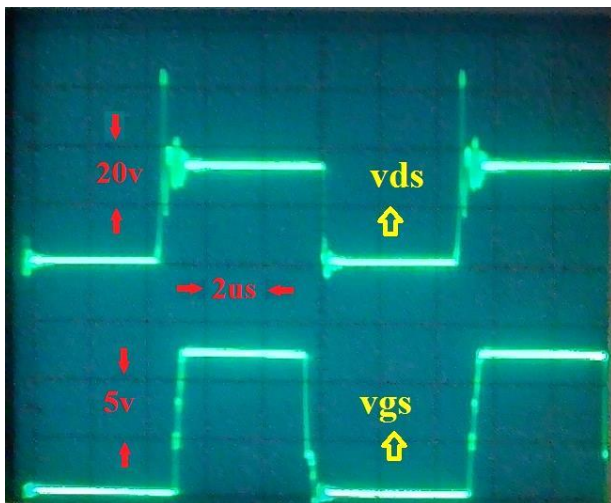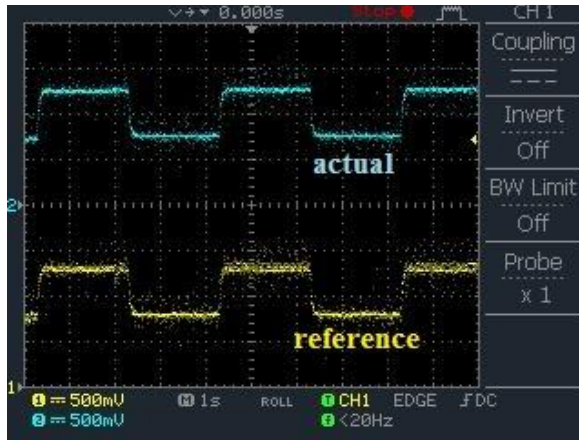

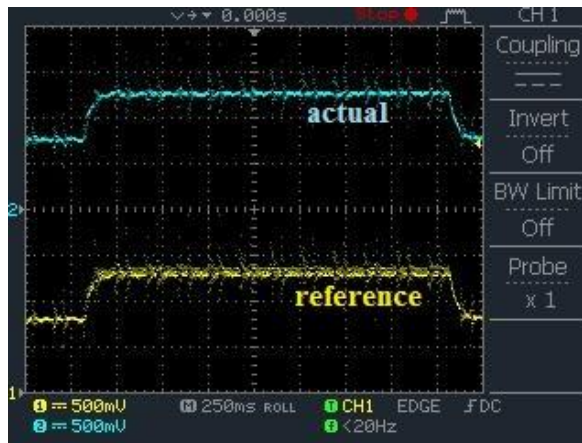
Fig. 10 – *Experimental setup.*

**Fig. 11 –** *Gate-source and drain-source voltages.*

(a)

(b)

Fig. 12 – *Load change:* (a) *currents;* (b) *currents zoomed*
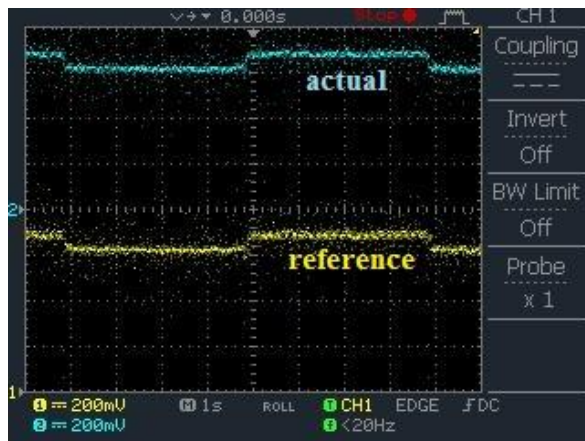(500 mV *is equivalent to* 0.5 A).

In the second test, the load is kept constant on 12.5 Ω or 2 5Ω and irradiation is changed between 1000 W/m² and 500 W/m² periodically. During this test the temperature is kept on 25 ºC. With the irradiation change, the PV characteristic curve is changed and the operation point is changed. The output current and its reference are represented in Fig. 13.

In the third test, again the load is kept constant on 12.5 Ω or 25 Ω; but this time, the temperature is changed between 25 ºC and 50 ºC periodically. During this test the irradiation is kept on 1000 W/m². With the temperature change, the PV characteristic curve is changed and the operation point is changed. The output

current and its reference are represented in Fig. 14. Compared to the results of Fig. 13 the changes in the reference current and consequently the actual output current are a little more which shows the correspondency to the PV characteristics. Using a more precise current sensor, better results can be obtained.
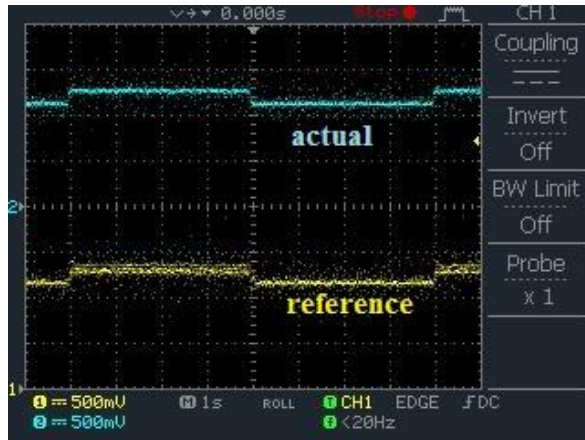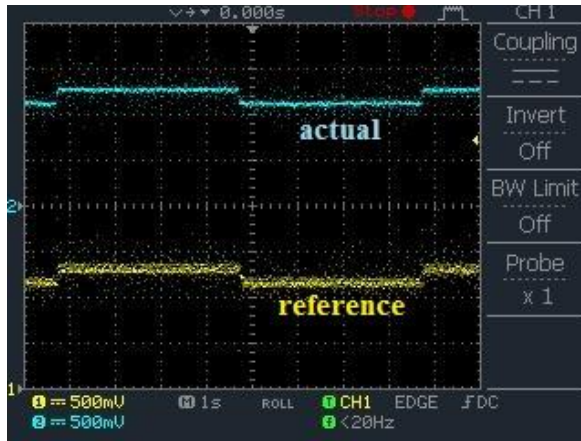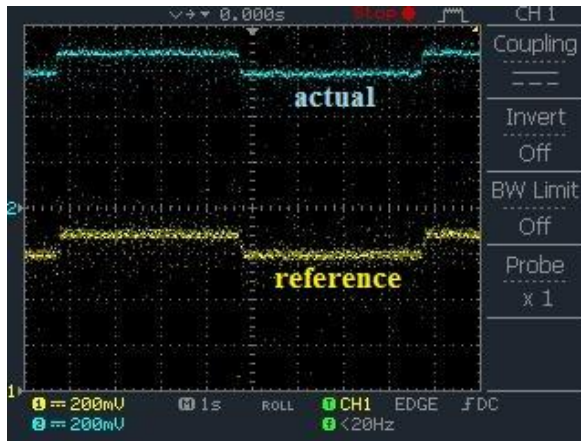

(a)

(b)

Fig. 13 – *Currents with irradiation change:* (a) *R* = 12.5 Ω*;*
(b) *R* = 25 Ω (500 mV *is equivalent to* 0.5 A).

(a)

(b)

Fig. 14 – *Currents with temperature change:* (a) $R = 12.5 \ \Omega$*;*
(b) $R=25\Omega$ (500 mV *is equivalent to* 0.5 A).

6   Conclusion

A PV module model is presented and validated by computer simulation and experimental results. The proposed model characterizes the nonlinear i–v curve of PV module with a very good accuracy and can be used for computer simulation or a practical digital PV module simulator. A switching DC-DC buck converter is employed to realize a PV module simulator using proposed model. Three simple effective (PI, SM and NTSM) controllers are proposed to realize PV module characteristics. The stability of the closed loop system and the stability

of the internal dynamic are investigated and proved. Computer simulations and experimental results show the validity and effectiveness of the proposed PV module simulator which can be used in researches needed PV modules with different temperatures and irradiations. The low cost proposed simulator is easily applicable in MATLAB/Simulink environment.

7   Acknowledgments

8   References

[1]   A. Chouder, S. Silvestre, N. Sadaoui, L. Rahmani: Modeling and Simulation of a Grid Connected PV System based on the Evaluation of Main PV Module Parameters, Simulation Modelling Practice and Theory, Vol. 20, No. 1, January 2012, pp. 46 – 58.

[2]   K. Ishaque, Z. Salam, H. Taheri, Syafaruddin: Modeling and Simulation of Photovoltaic (PV) System During Partial Shading based on a Two-Diode Model, Simulation Modelling Practice and Theory, Vol. 19, No. 7, August 2011, pp. 1613 – 1626.

[3]   J. Park, H.- G. Kim, Y. Cho, C. Shin: Simple Modeling and Simulation of Photovoltaic Panels Using Matlab/Simulink, Advanced Science and Technology Letters, Vol. 73, 2014, pp. 147 – 155.

[4]   D. Kapoor, P. Sodhi, D. Deb: Solar Panel Simulation Using Adaptive Control, Proceedings of the IEEE International Conference on Control Applications (CCA), Dubrovnik, Croatia, October 2012, pp. 1124 – 1130.

[5]   R. N. Tripathi, T. Hanamoto: Parameter Computation Using Circuit Based Approach for Two-Diode Model Based Solar PV Simulator with Partial Shading Effect, Proceeding of the 28th International Conference on Efficiency, Cost, Optimization, Simulation and Environmental Impact of Energy Systems (ECOS), Pau, France, June 2015, pp. 1 – 12.

[6]   A. S. Samosir: Modeling and Evaluation of Solar Photovoltaic Emulator based on SIMULINK Model, ARPN Journal of Engineering and Applied Sciences, Vol. 10, No. 22, December 2015, pp. 10288 – 10295.

[7]   S. Gupta, R. Avtar: Simulation and Modelling of Photovoltaic Power Conversion System, Proceedings of the International Conference on Recent Trends & Advancements in Engineering Technology (ICRTAET), Katra, India, May 2015, pp. 8 – 12.

[8]   M. A. Al-Refai: Matlab/Simulink Simulation of Solar Energy Storage System, Proceedings of the International Conference on Electrical, Computer and Communication Engineering, Barcelona, Spain, February 2014, pp. 297 – 302.

[9]   J. A. Ramos-Hernanz, J. J. Campayo, J. Larranaga, E. Zulueta, O. Barambones, J. Motrico, U. Fernandez Gamiz, I. Zamora: Two Photovoltaic Cell Simulation Models in MATLAB/SIMULINK, International Journal on Technical and Physical Problems of Engineering, Vol. 4, No. 10, March 2012, pp. 45 – 51.

[10] M. Karamirad, M. Omid, R. Alimardani, H. Mousazadeh, S. N. Heidari: ANN Based Simulation and Experimental Verification of Analytical Four and Five-Parameters Models of PV Modules, Simulation Modelling Practice and Theory, Vol. 34, May 2013, pp. 86 – 98.

[11] H. Lee, M.- J. Lee, S.- N. Lee, H.- C. Lee, H.- K. Nam, S.- J. Park: Development of Photovoltaic Simulator based on DC-DC Converter, Proceedings of the 31st International Telecommunications Energy Conference (INTELEC), Incheon, South Korea, October 2009, pp. 1 – 5.

[12] J. Zhang, S. Wang, Z. Wang, L. Tian: Design and Realization of a Digital PV Simulator with a Push-Pull Forward Circuit, Journal of Power Electronics, Vol. 14, No. 3, May 2014, pp. 444 – 457.

[13] D. Abbes, A. Martinez, G. Champenois, B. Robyns: Real Time Supervision for a Hybrid Renewable Power System Emulator, Simulation Modelling Practice and Theory, Vol. 42, March 2014, pp. 53 – 72.

[14] M. Luitel, M. Pokharel, G. Ojha: Design and Fabrication of Photovoltaic Simulator, Proceedings of the International Seminar on Solar Photovoltaic Systems: An Alternate Solution for the Growing Energy Demand, Dhulikhel, Nepal, November 2011, pp. 1 – 3.

[15] A. Nazar Ali, K. Premkumar, M. Vishnupriya, B. V. Manikandan, T. Thamizhselvan: Design and Development of Realistic PV Emulator Adaptable to the Maximum Power Point Tracking Algorithm and Battery Charging Controller, Solar Energy, Vol. 220, May 2021, pp. 473 – 490.

[16] A. Rachid, F. Kerrour, R. Chenni, H. Djeghloud: PV Emulator Based Buck Converter using dSPACE Controller, Proceedings of the IEEE 16th International Conference on Environment and Electrical Engineering (EEEIC), Florence, Italy, June 2016, pp. 1 – 6.

[17] W. Zhang, J. W. Kimball: DC-DC Converter Based Photovoltaic Simulator with a Double Current Mode Controller, IEEE Transactions on Power Electronics, Vol. 33, No. 7, July 2018, pp. 5860 – 5868.

[18] J.- J. Slotine, W. Li: Applied Nonlinear Control, Prentice-Hall, Englewood Cliffs, 1991.

[19] H. Sira-Ramírez, R. Silva-Ortigoza: Control Design Techniques in Power Electronics Devices, Springer, London, 2006.

[20] Y. Feng, X. Yu, Z. Man: Non-Singular Terminal Sliding Mode Control of Rigid Manipulators, Automatica, Vol. 38, No. 12, December 2002, pp. 2159 – 2167.

Appendix 1

Investigation of the convergence to sliding surface of NTSM control

Lemma 1. For system (20) with the sliding variable (21) and the NTSM control (24), if $\eta > |\Delta|_{max}$, then the reaching phase occurs in finite time.

Proof. Considering (22) – (24),

$$\dot{s} = y_2 + \beta^{-1} \frac{p}{q} y_2^{p/q-1} \left[f_1 + g_1 \left\{ \frac{\left[-\beta \frac{q}{p} y_2^{2-p/q} - f_1 + \dot{\bar{x}}_1 \right]}{g_1} - \eta \frac{\text{sign}(s)}{g_1} \right\} + \Delta - \dot{\bar{x}}_1 \right] \quad (26)$$

$$= \beta^{-1} \frac{p}{q} y_2^{p/q-1} \left[\Delta - \eta \text{sign}(s) \right],$$

then

$$s\dot{s} = \beta^{-1} \frac{p}{q} y_2^{p/q-1} \left[\Delta s - \eta \text{sign}(s)s \right] \leq$$

$$\leq -\beta^{-1} \frac{p}{q} y_2^{p/q-1} (\eta - |\Delta|_{max}) \, | \, s \, | = -\rho(y_2) \, | \, s \, |, \quad (27)$$

where

$$\rho(y_2) = \beta^{-1} \frac{p}{q} y_2^{p/q-1}(\eta - |\Delta|_{max}) \geq 0,$$

because $p/q - 1 = m/q$ and m is a positive even number.

From (27), it can be concluded that the sliding surface ($s = 0$) is an attractor and the convergence to it occurs in a finite time. For more details see [20].

Appendix 2

Investigation of the convergence to the origin for sliding phase of NTSM control

Lemma 2. For the sliding variable (21), the sliding phase occurs in finite time.

Proof. In the sliding phase the trajectories are on the sliding surface and considering (21), the system dynamics is given as

$$y_1 + \beta^{-1} y_2^{p/q} = 0, \tag{28}$$

or

$$\beta y_1^{q/p} + y_2 = 0, \tag{29}$$

Substituting for y_2 from (20) in (29), the following differential equation is obtained:

$$\dot{y}_1 + \beta y_1^{q/p} = 0, \tag{30}$$

Assume that the sliding phase starts at $t = 0$, the solution of (30) can be written as:

$$|y_1(t)| = \left[\left(\frac{y_1^{\frac{p-q}{p}}(0)}{\frac{p-q}{p}} - \beta t \right) \left(\frac{p-q}{p} \right) \right]^{\frac{p}{p-q}}, \tag{31}$$

Since p and q are positive odd numbers, $y_1^{\frac{p-q}{p}}(0) \geq 0$ and as time increases, $y_1(t)$ becomes zero at finite time $t = t_s$. Equating $y_1(t)$ from (31) to zero, gives

$$t_s = \frac{y_1^{\frac{p-q}{p}}(0)}{\beta\left(\frac{p-q}{p} \right)}. \tag{32}$$